Hybrid RANS-LES and URANS simulations of a laminar transonic airfoil

D. Szubert, F. Grossi, Y. Hoarau and M. Braza

Abstract

Laminar flow is a potential way of minimizing drag and reducing aircraft emissions. However, the interaction of laminar boundary layers with shock waves at transonic speeds can cause severe detrimental aerodynamic effects and remains an opened question. In this way, in the framework of the TFAST Project [1] – Transition Location Effect on Shock Wave Boundary Layer Interaction, a laminar transonic airfoil has been developed for both numerical and experimental studies on such laminar interactions. The so-called V2C profile has been designed to provide natural laminar flow from the leading edge to the shock wave for a wide range of freestream Mach numbers and angles of attack. In the present paper, a numerical investigation of the transonic flow around the V2C airfoil is conducted by means of URANS and hybrid RANS-LES computations. At sufficiently-high angles of attack and moderate freestream Mach numbers (0.70), the transonic interaction becomes unsteady, characterized by an oscillating shock wave arising from shock- induced separation. As the Mach number is further increased, the flow becomes fully separated with no shock motion. In the paper, special attention is paid to the differences between the URANS and hybrid RANS-LES predictions of shock-induced separation phenomena occurring over the V2C airfoil.

1 Introduction

Vision-2020, whose objectives include the reduction of emissions and a more effective transport systems, puts severe demands on aircraft velocity and weight. These

Y. Hoarau
ICube, Strasbourg, France, e-mail: hoarau@unistra.fr

D. Szubert, F. Grossi and M. Braza
Institut de Mécanique des Fluides de Toulouse, UMR 5502, France, e-mail: damien.szubert@imft.fr

require an increased load on wings and aero-engine components. The greening of air transport systems means a reduction of drag and losses, which can be obtained by keeping laminar boundary layers on external and internal airplane parts. Increased loads make supersonic flow velocities more prevalent and are inherently connected to the appearance of shock waves, which in turn may interact with a laminar boundary layer. Such an interaction can quickly cause flow separation, which is highly detrimental to aircraft performance and poses a threat to safety. In order to diminish the shock induced separation, the boundary layer at the point of interaction should be turbulent. In this context, the European research program TFAST (Transition Location Effect on Shock Wave Boundary Layer Interaction) was hosted, with the aim of studying the effects of transition location on the structure of the shock wave/boudary layer interaction, and several ways of controling the position of the transition, by the collaboration of European industrials as well as laboratories and universities. To this end, in the context of external flows, a supercritical laminar wing (the V2C) has been designed by Dassault Aviation. This profile allows the boundary layer to remain laminar up to the shock foot, even in the environment of transsonic wind tunnels of the laboratories involved in the project, and up to the angle of attack of 7°. Based on the natural flow developped around the profile, the laminar/turbulence transition can be imposed anywhere upstream the shock wave, and the effects of various locations can be studied. In precise ranges of Mach number and angle of attack, an airfoil in transonic regime can be submitted to a flow instability commonly known as transonic buffet. This unsteady shock wave/boundary layer interaction is considered as a self-sustained mechanism of low frequency shock oscillations of large amplitude, causing intense fluctuations of the aerodynamic forces. The structure, depending on its configuration, may submitted to vibrations from moderate to high amplitudes, causing lack of comfort, structure wear, tirgger aeroelastic flutter which may lead to rupture. This phenomenon has been studied experimentally in detail since the 70s [25, 29] on circular-arc airfoils, and most recently on supercritical airfoil [21]. The physics governing the transonic buffet is complex and still remains to be clarified, though several theories have been proposed, like the effect of the feedback mechanism of wave propagating from the trailing edge [22], or the onset a global instability [10].

Navier-Stokes simulations of transonic buffet as well as of the shock-vortex interaction at moderate Reynolds numbers were reported by Bouhadji and Braza [6, 7], as well as DNS by Bourdet et al [8]. While Computational Fluid Dynamics (CFD) techniques may provide considerably accurate results around the cruising design point of an airplane, for example, they become less reliable as one approaches the limits of the flight envelope, where nonlinear effects such as flow separation and shock waves get pronounced. Furthermore, the high Reynolds numbers typical of aerodynamic applications require the use of an appropriate closure for the turbulent stresses and time-resolved computations are frequently necessary. Concerning transonic buffet, the unsteady shock wave/boundary layer interaction represents a major challenge for turbulence models and the low frequencies associated with the shock-wave motion can make the simulations very expensive. Since the pioneering simulations by Levy [23] and Seegmiller et al. [29] for a circular-arc airfoil,

Unsteady Reynolds-Averaged Navier-Stokes (URANS) computations using eddy-viscosity turbulence models have been largely used to predict the phenomenon over two-dimensional airfoils, which is a model for the more complex airplane buffet problem [10]. Hybrid RANS-LES methods combine the robustness and near-wall physics offered by URANS in the near region, as well as LES capabilities of vortices and instabilities development in the detached flow regions, as for example in [12] capturing the buffet phenomeon around the OAT15A airfoil. Other recent applications can be found in the collected works after the 3rd and 4th Hybrid RANS-LES Symposia [27, 14]. Compared to standard RANS/URANS approaches where the turbulence spectrum is fully modeled, hybrid RANS-LES methods can provide extra level of physical representation through the resolution of part of the turbulent structures. Regarding their application to the transonic buffet problem, Grossi et al. [18] performed a Delayed Detached-Eddy Simulation (DDES) of the unsteady flow over the OAT15A supercritical airfoil that succeeded in predicting the self-sustained motion of the shock wave near the experimental buffet onset boundary. In the present paper, a similar strategy is applied on the V2C airfoil within the TFAST program, at 7°, the maximum angle of attack allowed by the design. A 2D study is first carried out to investigate the main characteristics of the airfoil regarding the effects of the angle of attack (section 4.1.1) as well as the influence of the turbulence model (section 4.1.2). The transition location effects are also studied in steady case and in the buffeting regime, by imposing the laminarity at several positions. These results are developped in section 4.1.3. The results of the 3D computations, URANS and DDES, are presented in the last section of this paper.

2 Flow configuration

The V2C profile has been specifically designed in the context of the TFAST project: the boundary layer needs to be laminar from the leading edge to the shock wave on the upper surface up to buffet onset. The technique employed for transition prediction was based on the e^N method (Ref. [11] for instance) and the airfoil surface was generated in such a way that the N-factor remains small for low-to-moderate turbulence intensity levels, such as in the wind tunnels used for that test case for the experimental study currently in progress. The design was validated numerically by Dassault on a 0.25 m-chord length (c) profile by means of RANS computations for various angles of attack at freestream Mach numbers of 0.70 and 0.75, yielding chord-based Reynolds numbers of approximately 3.245×10^6 and 3.378×10^6 respectively. The study was performed using a compressible Navier-Stokes code adopting a two-layer $k-\varepsilon$ model, with the transition location being determined from the fully-turbulent flowfield using a three-dimensional compressible boundary-layer code (see Ref. [9]) by means of the N-factor amplification with a parabola method (see Ref. [4]). The analysis of the flowfield around the airfoil indicated that the boundary layer is supposed to remain laminar up to the shock wave for angles of attack between 1° and 7°. At Mach 0.70, the flow separated between $\alpha = 6°$ and 7°.

The amplification factor N was shown to be smaller than 3 up to the shock wave, thus guaranteeing laminar flow. At Mach 0.75, the value of N remained smaller than 2 up to $\alpha = 7^\circ$. For this Mach number, there were not buffeting phenomenon, whatever the angle of attack. Moreover, for incidence higher than 1°, the shock induces a separation of the boundary layer until the trailing edge. These results are detailed in [16]). Only the results for the lowest Mach number will be presented here.

3 Numerical method and turbulence modelling

The simulations of the V2C configuration have been performed with the Navier-Stokes Multi-Block (*NSMB*) solver. The NSMB solver is the fruit of a european consortium that included Airbus from the beginning of 90s, as well as main European aeronautics research Institutes like KTH, EPFL, IMFT, ICUBE, CERFACS, Univ. of Karlsruhe, ETH-Ecole Polytechnique de Zurich, among other. This consortium is coordinated by CFS Engineering in Lausanne, Switzerland. NSMB solves the compressible Navier-Stokes equations using a finite volume formulation on Multi-Block structured grids. It includes a variety of efficient high-order numerical schemes and of turbulence modelling closures in the context of LES, URANS and of hybrid turbulence modelling. NSMB includes an ensemble of the most efficient CFD methods, as well as efficient fluid-structure coupling for moving and deformable structures. These developments can be found in [20] regarding URANS modelling for strongly detached flows, [24] in the area of moving body configurations, [5, 16, 19] allowing for Detached Eddy Simulation with the NSMB code. For the study presented here, the third-order of accuracy Roe upwind scheme [28] associated with the MUSCL van Leer flux limiter scheme [35] is used to discretize the convective fluxes. For the unsteady RANS, implicit time integration using the dual time stepping technique has been performed. A physical time step of 5 μs has been adopted for 2D simulations. For 3D calculation, the time step has been reduced to 0.1 μs. A typical number of inner iterations of 30 was necessary for the convergence in each time step. The methodology adopted in the simulations is the same as in [19].

The 2D planar grid has a C-H topology, and is of size 163,584 cells. The limit of the domain is located at a mean distance of 80 chords. A convergence study on the mesh refinement has been carried out, by means of steady computations (local time stepping) for the flow at $M_\infty = 0.70$ and $\alpha = 4.0^\circ$ using the Menter's SST model and assuming fully-turbulent behavior, with two others grids: one 50% coarser, and another 30% finer. Detailed results of this convergence study can be found in [16]. The grid retained for the present study gave a maximum value of non-dimensional wall distance y^+ of about 0.55 with respect to the turbulence modelling, near the wall. Figure 1 shows the grid and the computational domain.

For the 3D computations, the planar grid has been extruded to 59 cells uniformly distributed in the spanwise direction over a distance of $0.33 \times c$. The 3D grids contains about 9.65 M cells.

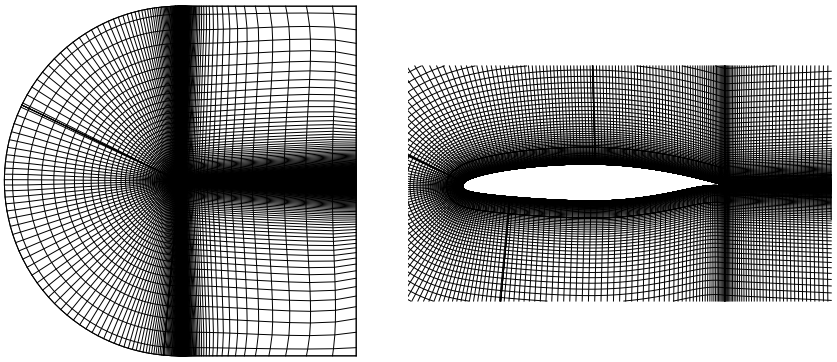

Fig. 1 Multiblock domain

Boundary conditions

On the solid wall, impermeability and no-slip conditions are employed. The far-field conditions are the characteristic variables extrapolated in time: the total pressure ($P_0 = 10^5 Pa$) and total temperature ($T_0 = 290$ K), as well as the upstream Reynolds number of 3.245 million and Mach number of 0.70. The upstream turbulence intensity is $Tu = 0.08\%$.

Turbulence modelling

Based on previous studies in our research group which examined the predictive ability of various turbulence models [15, 17, 19] regarding transonic flow field, in steady case as well as unsteady (transonic buffeting), the two-equation $k-\omega$ SST model of Menter [26] with turbulence-sustaining ambiant terms to prevent the free decay of the transported turbulence variables [34] has been used for the (U)RANS and the DDES computations.

4 Results

4.1 Two-dimensional study

4.1.1 Effects of the angle of attack

In order to characterize the aerodynamics of the V2C airfoil at $M_\infty = 0.70$, the angle of attack is varied from 1° up to 7°, which is the maximum angle of attack for which

the boundary layer is supposed to remain laminar from the leading edge to the shock wave. Initially, the computations adopt local time stepping. If convergence is not reached (i.e., a relative reduction of 10^{-6} in the residual), time-accurate simulations with a time step of $5 \times 10^{-6} s$ are then performed. Near the critical angle regarding the buffet, the angle of attack is varied by an increment of 0.5° in order to refine the buffet boundary.

Figure 2 shows the final distributions of the pressure coefficient for the full range of incidences and the skin-friction coefficient for the steady cases. For angles of attack up to 5°, the flow is steady and rear separation is always present. The shock wave can already be distinguished at 2°. As the angle of attack is further increased, the shock initially moves downstream, then it goes upstream for $\alpha > 3^\circ$. From $\alpha = 4^\circ$, a bubble separation appears and develops, and the amount of rear separation steadily increases with the angle of attack (fig. 2(b)).

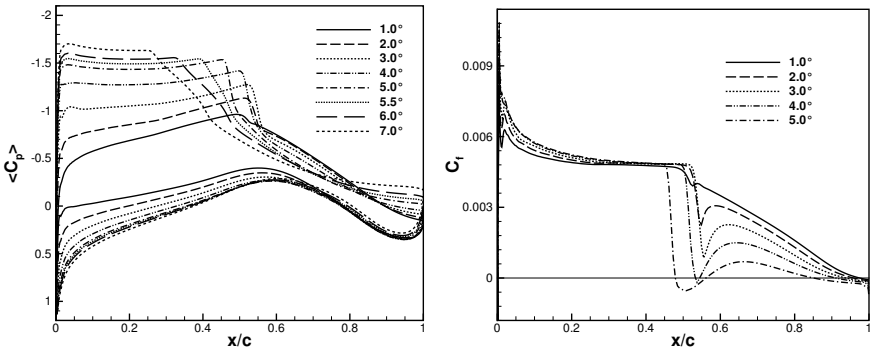

(a) Pressure coefficient (b) Friction coefficient

Fig. 2 Steady and mean surface distributions

Flow unsteadiness, characterized by an oscillating shock wave, has been detected from 5.5°. The main frequency increases with incidence in the range of $80-82$ Hz. At 5.5° the amplitude of the shock-wave motion is still small, resulting in a slight slope in the C_p curve. The buffet phenomenon seems to be fully established at 6° as the shock-motion range and the maximum fluctuation levels in the shock region and near the trailing edge (fig. 3) are very similar to the case $\alpha = 7^\circ$. For the latter, the whole SWBLI is somewhat shifted upstream, yielding a shorter supersonic plateau and a larger separation region.

It has to be mentioned that the experimental study of this flow configuration was just started within TFAST. For this reason, comparison with experiments are not yet available. However while this results have been obtained using one numerical solver, they have been compared to another code, Edge ([2, 3]), an unstructured compressible finite volume CFD code developed by the FOI since 1997 in collaboration with industrial and academic partners. This comparison showed small differences closed

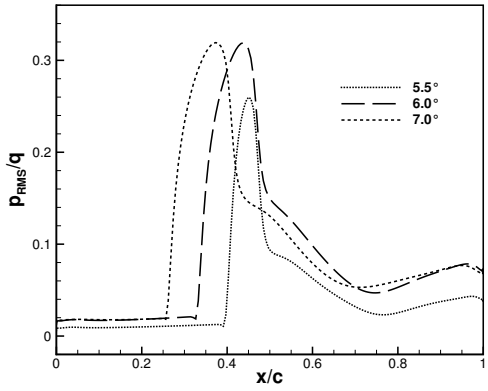

Fig. 3 RMS value of the pressure on the upper surface

to the critical angle, but the results were very similar at lower and higher angles of attack.

In the next section, these results are compared to the same calculations performed in (U)RANS based on the Spalart-Allmaras turbulence model.

4.1.2 Influence of the turbulence model

The sensitivity of the critical angle to the buffet phenomenon at Mach number 0.70 has been studied in terms of the turbulence models used in the 2D URANS calculations. Results from the two-transport equations $k-\omega$ SST turbulence model presented in the previous section, are compared to those obtained by the Edwards and Chandra variant [13] of the one-equation model of Spalart-Allmaras [32], using the compressibility correction of Secundov [30, 31] (SAE+CC). The mean surface pressure coefficient is plotted in figure 4 at the angles of attack of 4° and 5°. At the lowest incidence (figure 4(a)), below the critical angle, the modified Spalart-Allmaras gives a steady position of the shock wave downstream than with the $k-\omega$ SST model.

The modified Spalart-Allmaras model reaches the critical angle of $\alpha = 5.0°$ whereas, as seen in the previous section, the onset of the buffeting phenomenon appeared at an angle of $\alpha = 5.5°$ for the $k-\omega$ SST model.

4.1.3 Transition study

Two flow conditions have been selected for a numerical investigation of the transition location effect on the shock wave/boundary layer interaction, due to their interesting flow physics. First, the steady interaction arising at $\alpha = 4.0°$ is addressed, featuring a reasonably strong shock just below the critical angle of attack for buffet

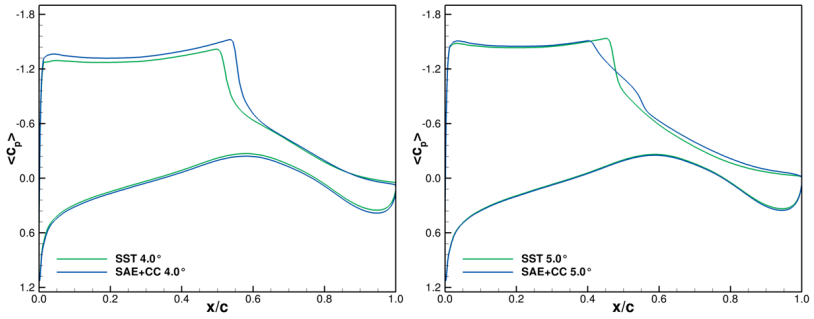

(a) AoA = 4° (b) AoA = 5°

Fig. 4 Comparison of mean pressure coefficient distribution for $k-\omega$ SST and Spalart-Allmaras models at incidences 4° and 5°

onset. The second flow condition is the fully-established buffet regime at $\alpha = 7.0°$, which presents a large shock-wave motion region.

The transition is forced at the position x_t by imposing the turbulent viscosity $\nu_t = 0$ for $x < x_t$. Its location x_t is varied from the leading edge up to as close as possible to the shock wave, providing long extents of laminar boundary layer upstream it. The influence of the tripping point over the selected steady and unsteady transonic flowfields is presented in the following two sections.

Pre-buffet condition – Steady case

Results presented in the previous sections showed that, at $\alpha = 4.0°$ and $M_\infty = 0.70$, the fully turbulent flow over the V2C airfoil is near critical with respect to transonic buffet. At that incidence, the shock wave is strong enough to induce a small separation bubble and the adverse pressure gradient over the rear part of the airfoil causes rear separation at about $x/c = 0.91$. The same flow condition has been recomputed considering different transition locations x_t from the leading edge up to the mid-chord, remaining steady in all cases. The pressure and friction coefficients distributions over the upper surface are plotted in figure 5 for some chosen values of x_t. The effect of the transition location on the shock-wave position x_s, on the location x_b and length l_b of the separation bubble as well as on the rear separation position x_r are detailed in table 1 for the complete set of simulations.

The tripping points can be easily identified on the friction coefficient by the sudden and high increase in the wall shear when the boundary layer becomes turbulent. They can also be distinguished on the pressure coefficient in the form of slight pressure disturbances in the supersonic region. As the transition location is shifted downstream, which induced a reduction in the boundary layer displacement thickness, the shock wave moves downstream, which can be noted in the figures. This produces higher Mach number levels in the supersonic pocket associated with lower pressures in that region, resulting in a stronger compression through the shock. As the laminar region increases, the progressively stronger shock wave makes the sep-

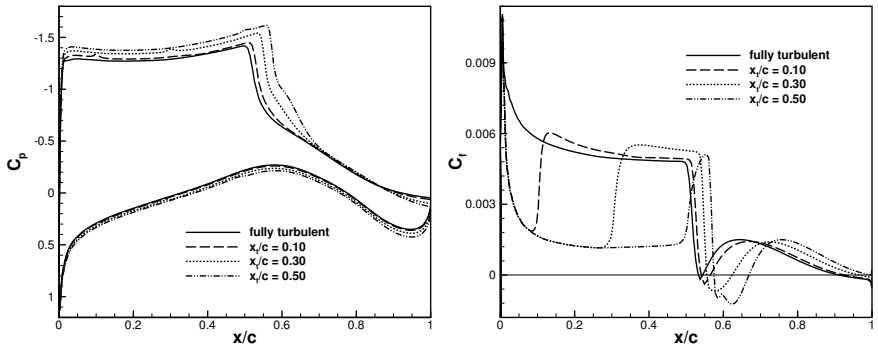

(a) Pressure coefficient (b) Friction coefficient

Fig. 5 Steady surface distributions for selected transition locations

aration bubble grow continuously as indicated in table 1 and by means of the C_f distribution. On the contrary, the rear separation gets smaller, yielding a larger pressure recovery and eventually vanishing for $x_t/c \approx 0.5$.

Table 1 provides also the force coefficients as the tripping point is varied. As the length of the laminar region, and thus the shock wave position move downstream, the lift increases due to a higher pressure difference between the upper and lower surfaces. The lift-to-drag ratio L/D is also provided. An optimal value is found near $x_t/c = 0.3$. However, this position of transition does not give the minimum value of the global drag coefficient, which is obtained for a transition located near $x_t/c = 0.10$, with a short laminar boundary layer region. This drag coefficient then increases with a longer laminar region, while the friction drag always diminishes as the laminar region gets longer.

x_t/c	fully turb.	0.10	0.20	0.30	0.40	0.50
x_s/c	0.523	0.532	0.541	0.552	0.564	0.574
x_b/c	0.533	0.541	0.547	0.556	0.566	0.575
l_b/c (%)	1.1	2.4	4.7	6.8	8.5	9.4
x_r/c	0.911	0.925	0.946	0.965	0.981	–
C_L	0.8873	0.9174	0.9556	0.9919	1.029	1.061
$C_{D_f} \times 10^2$	0.610	0.574	0.510	0.460	0.396	0.334
$C_D \times 10^2$	2.080	2.069	2.102	2.171	2.268	2.365
L/D	42.7	44.3	45.5	45.7	45.4	44.9

Table 1 Transition location effect on the shock position, on separation and on the global aerodynamic coefficients

Unsteady regime

This study has been carried out to assess the influence of the transition point on the properties of the well-developed buffeting flow at 7°. Besides the fully-turbulent

case, three tripping locations have been considered: $x_t/c = 0.09$, 0.16 and 0.24. For the latter, the most upstream position of the shock wave during buffet has been of about $x_t/c = 0.25$. This limits the displacement of the tripping point since imposing $\nu_t = 0$ inside the shock-motion region would not be an acceptable approximation.

Figure 6(a) presents the statistical pressure distributions obtained for each boundary layer tripping position. While the most upstream limit of the shock-motion range is not much sensitive to the transition location, its most downstream limit is strongly affected by the boundary layer state. As seen for the case $\alpha = 4^\circ$, a larger extent of laminar boundary layer tends to move the shock wave further downstream by altering the displacement thickness distribution around the airfoil. In fact, this effect can also be observed in the unsteady case regarding the mean shock-wave position, which roughly corresponds to the point of maximum pressure unsteadiness in figure 6(b). As the tripping point is placed downstream, the amplitude of shock motion becomes wider, increasing the fluctuation levels in the shock-wave region as well as the trailing edge unsteadiness. This can be observed in the series presented in figure 7, in terms of statistical pressure fluctuation fields. Comparing to the fully-turbulent simulation with the most laminar case ($x/c = 0.24$), the pressure unsteadiness increases by approximately 20% in the shock region and gets nearly two times larger near the trailing edge. The development of the shock-motion area as a function of the transition location is clearly visible in figure 7/

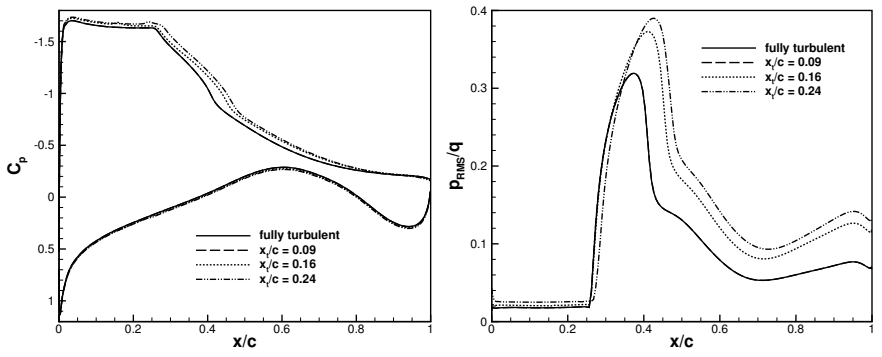

(a) Mean pressure coefficient (b) RMS value of pressure on the upper surface

Fig. 6 Statistical wall pressure at $\alpha = 7.0^\circ$

Table 2 gives the average lift, drag and pitching moment coefficients for the three transition cases as well as for the fully-turbulent computation. The standard deviation σ of the aerodynamic forces is also presented. As for the steady flow at 4°, the values of the mean lift and of the moment magnitude inscrease as the triggering location moves towards the trailing edge. A slight augmentation in the mean drag is also noticed. As a result of the increasing shock-motion amplitude and of the overall flow unsteadiness, the standard deviations of the lift and drag coefficients also become larger as the extent of laminar boundary layer gets longer. Therefore the

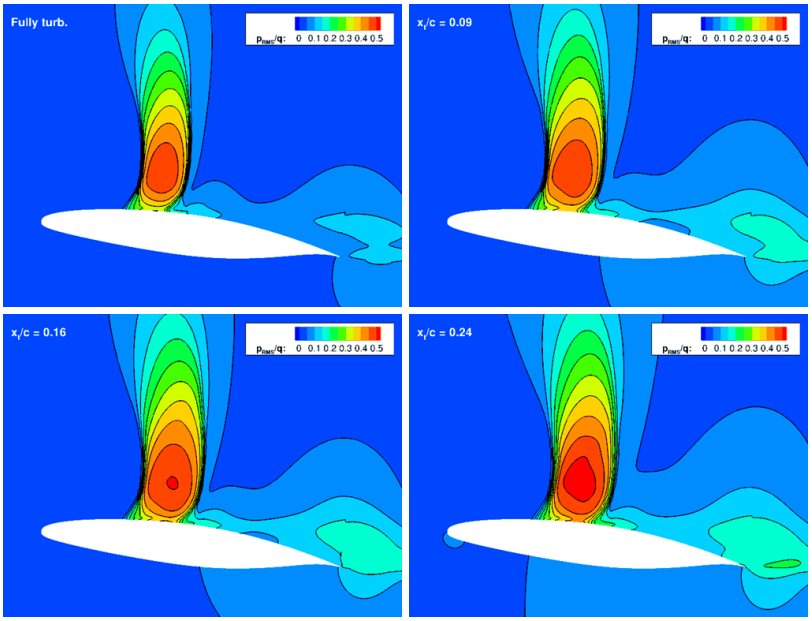

Fig. 7 RMS pressure fields for different transition locations at $\alpha = 7.0^\circ$

mean lift over mean drag ration doesn't show much improvement whereas the laminar region is inscreased. Indeed, as the transition is located closer to the shock wave/boundary layer interaction, the boundary layer downstream detaches more easily than the fully-turbulent case, which gave here the higher lift-to-drag ratio. Moreover, due to the high angle of attack, the most upstream location of the shock is near 25% of the chord, which limits the flexibility on the position of the transition.

x_t/c	Fully turb.	0.09	0.16	0.24
$\overline{C_D} \times 10^2$	6.163	6.501	6.604	6.715
$\sigma(C_D) \times 10^2$	0.9419	1.250	1.384	1.533
$\overline{C_L}$	0.9423	0.9718	0.9927	1.018
$\sigma(C_L)$	0.0854	0.1047	0.1132	0.1204
$\overline{C_m} \times 10^2$	-4.223	-4.932	-5.267	-5.676
$\overline{C_L}/\overline{C_D}$	15.3	14.9	15.0	15.2

Table 2 Transition location effect on the unsteady global coefficients

4.2 Three-dimensional simulation of the fully-turbulent case

4.2.1 DDES

The Delayed Detached-Eddy Simulation approach was also used in [16, 19] to simulate the transonic flow over the OAT15A supercritical airfoil at conditions of angle of attack just above the buffet onset boundary. In that case, the predicted shock-wave motion region was in good agreement with the experiments and the solution exhibited a rich content of resolved flow structures. Nevertheless, probably due to a long delay in the formation of resolved structures in LES regions, the DDES was shown to produce too-intense pressure and velocity fluctuations in the region downstream the oscillating shock wave.

In this study, the DDES method is applied, based on similar numerical configuration (same numerical scheme and time step $\Delta t = 10^{-7}s$), to the well-developed transonic buffet occurring over the V2C airfoil at $M_\infty = 0.70$ and $\alpha = 7.0°$. The objective is to investigate whether the same issues detected in the OAT15A test case exist for a stronger shock-induced separation by comparing the DDES results with those of the previous URANS simulation. Due to the high computational cost of the simulation and for simplicity, only the fully-turbulent configuration is considered. The three-dimensional grid has been obtained by copying the planar grid used in the URANS simulations in the spanwise direction over a distance $L_z/c = 0.33$. To obtain $\Delta i \approx \Delta k$, 59 cells have been distributed along the span keeping a constant spacing, resulting in a final grid of about 9.65 M cells.

In the SST-based DDES, the turbulence length scale provided by the RANS part is computed using local turbulence properties and is given by $\sqrt{k}/(\beta^* \omega)$.

Flowfield dynamics

The time history of lift after the transient period is presented in figure 8 for both the DDES and the fully-turbulent 2D URANS computation. While in URANS the lift coefficient oscillates quasi-harmonically at a frequency of approximately 82 Hz, the DDES produces non periodical sharp and much stronger lift fluctuations. The high slope of the curve indicates that the shock-wave speed is relatively high, especially during the lift fall when the flow separates and the shock moves upstream. This may explain, at least partially, the somewhat higher mean buffet frequency found in that case (approximately 106 Hz). The large amplitude of the fluctuations suggests also that the shock-wave motion range is wider than in URANS.

A series of flow snapshots is presented in figure 9 for one period of buffet. It helps understanding the dynamics of the flow predicted by the DDES. The figures illustrate instantaneous isosurfaces of non-dimensional vorticity magnitude for $|\overrightarrow{\omega}|c/U = 10$ as a function of the non-dimensional time $t^* = tU/c$, where $t^* = 0$ is an instant of maximum lift. Surfaces are colored with the Mach number. During the upstream travel of the shock (figures 9(a)), alternate vortex shedding can be observed at the trailing edge. The primary structures are always three-dimensional. As the shock approaches the leading edge, the flow over the upper surface gets fully

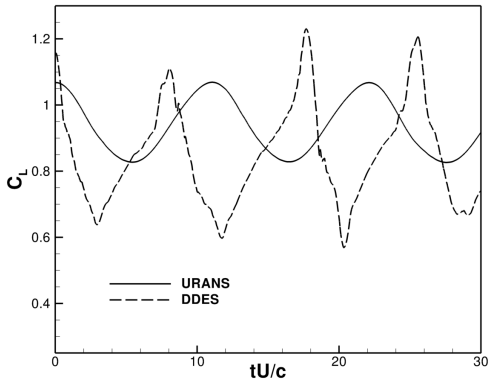

Fig. 8 Time history of lift at $M_\infty = 0.70$ and $\alpha = 7.0^\circ$

separated and the shear layer becomes unstable (figures 9(b) and 9(c)). Such intense separation generates a large wake combining the eddies produced in the shear layer and the trailing edge structures. As the shock and the separation point move downstream, the height and streamwise extension of the separation region decrease and the amount of resolved flow structures reduces as seen in the sequence in the figures 9(d) and 9(e). Unlike in URANS, a considerable amount of separation always exists on the rear part of the airfoil. While the shear layer becomes stable as the shock wave approaches its most downstream position, the alternate vortex shedding at the trailing edge is always present during buffet (figures 9(f)).

The distribution of the RANS and LES has been monitored in order to evaluate the ability of the present SST-based DDES to switch between the two modes during buffet. This analysis shows the existence of a RANS-mode layer covering the near-wall region around the V2C airfoil. The overall height of this layer seems to be relatively small. This might cause some degree of modeled-stress depletion [33] due to the erroneous penetration of the LES mode into attached boundary layers, which facilitates separation. The instantaneous distributions of the function $1 - f_d$ at four phases of buffet are given in figure 10. The irregular black areas over the upper surface indicate large regions of separation, even when the shock is at its most downstream position (fig. 10(d)) where a large amount of rear separation exists on the upper surface. It should be remembered that the hybrid method used here is originally intended to massively separated flows so that the present application should be regarded as an extended use of DDES as the height of the separation region remains small during buffet.

Statistical flow properties

The differences between DDES and URANS simulations in terms of mean pressure distributions, plotted in figure 11(a), are important. The shock wave and thus the separation point reach the leading edge in their travel upstream, as indicated by the lack of a supersonic plateau in the DDES. The shock-motion range is much

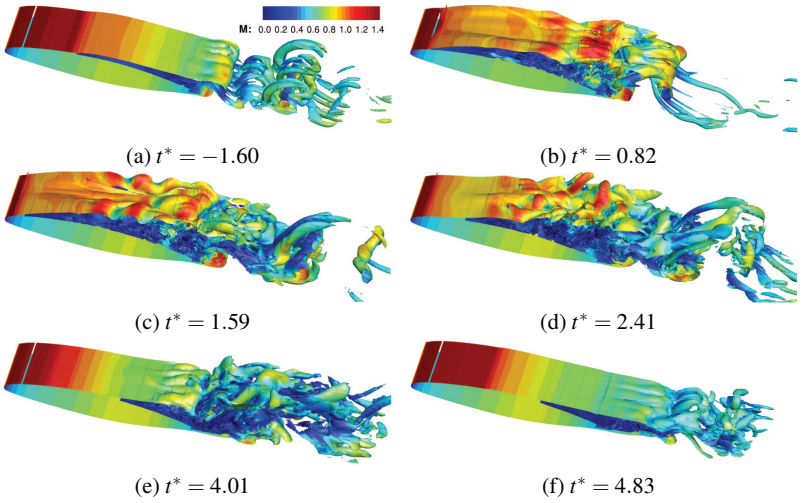

(a) $t^* = -1.60$ (b) $t^* = 0.82$

(c) $t^* = 1.59$ (d) $t^* = 2.41$

(e) $t^* = 4.01$ (f) $t^* = 4.83$

Fig. 9 Instantaneous vorticity magnitude isosurfaces for $|\vec{\omega}|c/U = 10$

(a) Maximum lift ($t^* = 0$) (b) Shock upstream ($t^* = 1.46$)

(c) Minimum lift ($t^* = 2.96$) (d) Shock downstream ($t^* = 6.02$)

Fig. 10 RANS and LES regions around the V2C airfoil

wider than in URANS, covering about 40% of the chord, and the flattened aspect downstream the shock-motion region suggests the occurrence of a large amount of separation. The RMS pressure distributions show in figure 11(b) thant the maximum unsteadiness levels in the shock region are lower than in the URANS computations, whereas over the rear part of the airfoil, the pressure fluctuations predicted by the DDES are much higher. This result suggests that, the delay in the development of resolved flow structures in the shear layer and in the separated region arising from the 'gray area' is critical in DDES, even in this case of shock-induced separated flows at relatively high angles of attack. The RMS fields of the velocity components (fig 12) lead to similar interpretation. The longitudinal components shows large differences between the two types of computations in the amplitude of the shock-wave motion and in the unsteadiness of the separated region. The discrepancies at the trailing edge are large, being primarily caused by alternate vortex structures, can been seen

by the transversal component of the velocity. Although such phenomenon might indeed exist, its strength and stability is probably overestimated in the simulation.

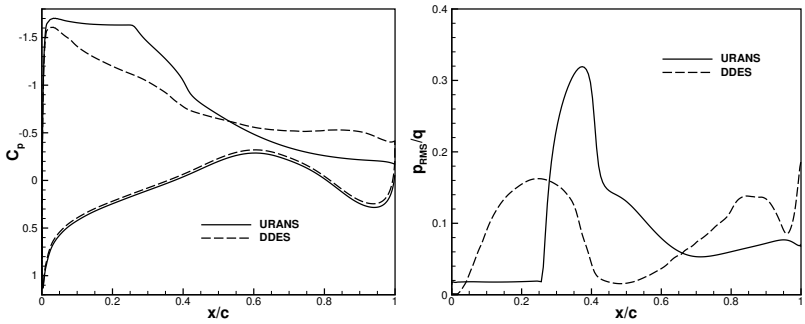

(a) Mean pressure coefficient (b) RMS pressure on the upper surface

Fig. 11 URANS and DDES statistical pressure distributions at $M_\infty = 0.70$ and $\alpha = 7.0°$

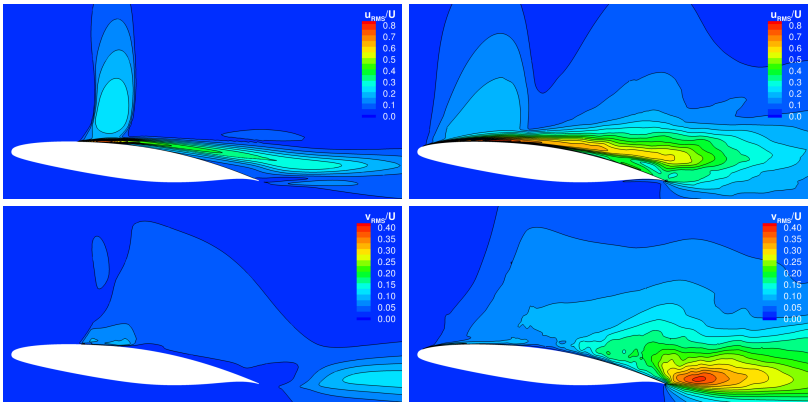

(a) URANS (b) DDES

Fig. 12 RMS value of longitudinal (top) and vertical (bottom) velocity fields around the V2C airfoil

4.3 Three-dimensional URANS

Based on the results of the DDES simulations detailed in the previous section, a new set of computations have been carried out on a grid which has 30% more cells in

A revoir

all directions, leading to grid of about 23 M cells, with the hope to evaluate more accurately the limit between the RANS and LES. Two 3D URANS computations are performed. One is based the Edwards and Chandra's variant [13] of the Spalart-Allmaras turbulence model [32] with the Secundov's compressibility correction [30] as suggested by Spalart [31] to improve the behavior of the one-equation model in compressible mixing layers. The other uses the $k-\omega$ SST model [26] with ambiant terms [34], as in all the results presented until now (except for the effects of the turbulence model studied in section 4.1.2).

Lift coefficient is plotted in the figure 13 of the transient phase, in addition to the results obtained with the previous grid. On the one hand, amplitudes of the lift coefficient from the Spalart-Allmaras simulation are large and have a low frequency compared to the full established buffet regime in 2D. On the other hand, the variations of the lift for the $k-\omega$ SST (values on the right vertical axis) are extremely low.

These computations need to be continued to confirm the tendency of the results, and the hybrid method needs to be applied and compared with those presented in this study.

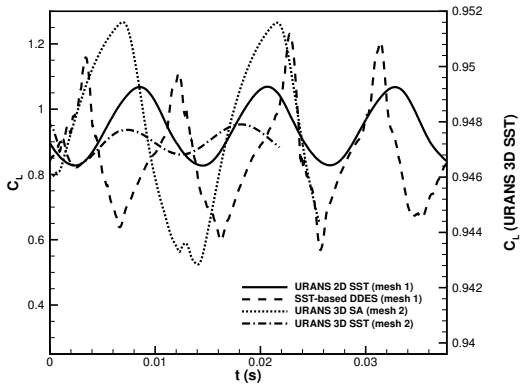

Fig. 13 Comparison of lift coefficient for the latest computations

5 Conclusion

The transonic V2C profile has been first investigated in terms of 2D (U)RANS computations. The different flow phenomena occurring around the airfoil for various angles of attack at Mach number 0.70 have been analysed. Pressure and skin friction distribution have shown the effects of the angle of attack on the shock wave position, as well as on the state of the boundary layer and its interaction with the

foot of the shock. The critical angle regarding the transonic buffet onset has been found to be dependent on the turbulence closure model: while the Spalart-Allmaras model gave a critical angle of 5°, the onset of the buffeting phenomenon appeared at a higher angle, 5.5°, for the $k-\omega$ SST model. The study of the influence of the transition location effect has been carried out in a steady case, first at an angle of attack of 4°, by varying the transition from $x/c = 0$ to 50% of the chord. Here again the effects on the pressure distribution and on the skin friction, as a function of the transition location, have been analysed. In particular, the global drag diminishes when a small laminar region (10% of the chord) is imposed but then increases, giving an optimal lift-drag ratio for a tripping position of $x/c = 0.3$. The unsteady case, in the buffeting conditions (angle of attack of 7°) has been analysed with the same method, for a maximum downstream position of the transition at $x/c = 0.24$, due to the shock motion. The increase of RMS pressure within the shock-wave region and downstream the SWBLI region, downstream the interaction, have been shown. A hybrid RANS-LES simulation has been also performed for the transonic buffet over the V2C airfoil at a relatively high angle of attack, where the flow is supposed to give a more wide detached area. The DDES approach has been used with the SST model in the RANS part. The results exhibited a rich content of resolved flow structures. Nonetheless, the DDES predictions were very different from the URANS simulations. This included the mean shock location and amplitude of the shock-wave oscillations, which indicated that the shock reached the leading edge during buffet in the hybrid case. Overall, the RANS-mode layer around the airfoil was relatively thin, which may have caused some degree of MSD and thus facilitated separation. Furthermore, in DDES, the pressure and velocity fluctuations over the rear part of the airfoil were much higher than in URANS. This result suggests the gray area issue as critical, despite the higher incidence and the existence of more eddies in the flowfield. Consequently to these results, a new set of 3D computations are currently carried out by means of URANS and DDES simulation on a 30% finer grid. Preliminary URANS results have been presented, revealing differences compared to the previous simulations on the initial grid, where the SST model is found to damp the buffet oscillations by using the finer grid.

Acknowledgements CINES
Calmip

References

1. URL www.tfast.eu
2. Edge Theoretical Formulation. FOI dnr 03-2870 5.2. FOI (2011)
3. Edge User Guide. FOI dnr 03-2870 5.2. FOI (2011)
4. Arnal, D.: Boundary layer transition: Prediction, application to drag reduction. AGARD-R-786, Special Course on Skin Friction Drag Reduction, AGARD (1992)
5. Barbut, G., Braza, M., Hoarau, Y., Barakos, G., Sévrain, A., Vos, J.B.: Prediction of transonic buffet around a wing with flap. In: Progress in Hybrid RANS-LES Modelling, pp. 191–204. Springer (2010)

6. Bouhadji, A., Braza, M.: Organised modes and shock–vortex interaction in unsteady viscous transonic flows around an aerofoil: Part I: Mach number effect. J. Computers & Fluids **32**(9), 1233–1260 (2003)
7. Bouhadji, A., Braza, M.: Organised modes and shock–vortex interaction in unsteady viscous transonic flows around an aerofoil: Part II: Reynolds number effect. J. Computers & Fluids **32**(9), 1261–1281 (2003)
8. Bourdet, S., Bouhadji, A., Braza, M., Thiele, F.: Direct numerical simulation of the three-dimensional transition to turbulence in the transonic flow around a wing. Flow, Turbulence and Combustion **71**(1-4), 203–220 (2003)
9. Courty, J.C., Bulgubure, C., Arnal, D.: Laminar flow investigation: Computations and flight tests at dassault aviation. AGARD-CP-547, Recent Advances in Long Range and Long Endurance Operation of Aircraft, AGARD (1993)
10. Crouch, J.D., Garbaruk, A., Magidov, D., Travin, A.: Origin of transonic buffet on aerofoils. Journal of Fluid Mechanics **628**, 357–369 (2009)
11. Crouch, J.D., Ng, L.L.: Variable *N*-factor method for transition prediction in three-dimensional boundary layers. AIAA journal **38**(2), 211–216 (2000)
12. Deck, S.: Numerical computation of transonic buffet over a supercritical airfoil. AIAA Journal **43**(7), 1556–1566 (2005)
13. Edwards, J.R., Chandra, S.: Comparison of eddy viscosity-transport turbulence models for three-dimensional, shock-separated flowfields. AIAA Journal **34**(9), 756–763 (1996)
14. Fu, S., Haase, W., Peng, S.H., Schwamborn, D. (eds.): Progress in Hybrid RANS-LES Modelling, *Notes on Numerical Fluid Mechanics and Multidisciplinary Design*, vol. 117. Springer (2012). Papers Contributed to the 4th Symposium on Hybrid RANS-LES Methods, Beijing, China, September 2011
15. Grossi, F.: Simulation numérique et analyse physique du tremblement transsonique d'un profil supercritique par approche de modélisation de la turbulence statistique avancée. Master's thesis, IMFT (2010)
16. Grossi, F.: Physics and modeling of unsteady shock wave/boundary layer interactions over transonic airfoils by numerical simulation. Ph.D. thesis, INP Toulouse (2014)
17. Grossi, F., Braza, M., Hoarau, Y.: Simulation numérique et analyse physique du tremblement transsonique d'un profil supercritique à reynolds élevé. 20ème Congrès Français de Mécanique (2011)
18. Grossi, F., Braza, M., Hoarau, Y.: Delayed detached-eddy simulation of the transonic flow around a supercritical airfoil in the buffet regime. In: S. Fu, W. Haase, S.H. Peng, D. Schwamborn (eds.) Progress in Hybrid RANS-LES Modelling, *Notes on Numerical Fluid Mechanics and Multidisciplinary Design*, vol. 117, pp. 369–378. Springer (2012)
19. Grossi, F., Braza, M., Hoarau, Y.: Prediction of transonic buffet by delayed detached-eddy simulation. AIAA Journal (2013). DOI 10.2514/1.J052873
20. Hoarau, Y.: Analyse physique par simulation numérique et modélisation des écoulements décollés instationnaires autour de surfaces portantes. Ph.D. thesis, INPT (2002)
21. Jacquin, L., Molton, P., Deck, S., Maury, B., Soulevant, D.: Experimental study of shock oscillation over a transonic supercritical profile. AIAA Journal **47**(9), 1985–1994 (2009). Also AIAA Paper 2005–4902, jun. 2005
22. Lee, B.H.K., Tang, F.C.: Transonic buffet of a supercritical airfoil and trailing-edge flap. Journal of Aircraft **26**(5), 459–464 (1989)
23. Levy Jr., L.L.: Experimental and computational steady and unsteady transonic flows about a thick airfoil. AIAA Journal **16**(6), 564–572 (1978)
24. Martinat, G., Braza, M., Hoarau, Y., Harran, G.: Turbulence modelling of the flow past a pitching NACA0012 airfoil at 10^5 and 10^6 Reynolds numbers. Journal of Fluids and Structures **24**(8), 1294–1303 (2008)
25. McDevitt, J.B., Levy Jr., L.L., Deiwert, G.S.: Transonic flow about a thick circular-arc airfoil. AIAA Journal **14**(5), 606–613 (1976)
26. Menter, F.R.: Two-equation eddy-viscosity turbulence models for engineering applications. AIAA Journal **32**(8), 1598–1605 (1994)

27. Peng, S.H., Doerffer, P., Haase, W. (eds.): Progress in Hybrid RANS-LES Modelling, *Notes on Numerical Fluid Mechanics and Multidisciplinary Design*, vol. 111. Springer (2010). Papers Contributed to the 3th Symposium on Hybrid RANS-LES Methods, Gdansk, Poland, June 2009
28. Roe, P.L.: Approximate riemann solvers, parameter vectors, and difference schemes. Journal of Computational Physics **43**(2), 357–372 (1981)
29. Seegmiller, H.L., Marvin, J.G., Levy Jr., L.L.: Steady and unsteady transonic flow. AIAA Journal **16**(12), 1262–1270 (1978)
30. Shur, M., Strelets, M., Zaikov, L., Gulyaev, A., Kozlovand, V., Secundov, A.: Comparative numerical testing of one- and two-equation turbulence models for flows with separation and reattachment. AIAA Paper (95-0863) (1995)
31. Spalart, P.R.: Trends in turbulence treatments. AIAA Paper 2000-2306 (2000)
32. Spalart, P.R., Allmaras, S.R.: A one-equation turbulence model for aerodynamic flows. La Recherche Aérospatiale **1**, 5–21 (1994)
33. Spalart, P.R., Deck, S., Shur, M.L., Squires, K.D., Strelets, M.K., Travin, A.: A new version of detached-eddy simulation, resistant to ambiguous grid densities. Theor. Comput. Fluid Dyn. (20), 181–195 (2006)
34. Spalart, P.R., Rumsey, C.L.: Effective inflow conditions for turbulence models in aerodynamic calculations. AIAA Journal **45**(10), 2544–2553 (2007)
35. van Leer, B.: Towards the ultimate conservative difference scheme. V. A second-order sequel to Godunov's method. Journal of Computational Physics **32**(1), 101–136 (1979)